Cellulose (2014) 21:2247–2259
DOI 10.1007/s10570-014-0262-y

ORIGINAL PAPER

Proton mobility and copper coordination in polysaccharide- and gelatin-based bioblends and polyblends

R. I. Mattos · C. E. Tambelli · E. Raphael · I. D. A. Silva · C. J. Magon · J. P. Donoso · A. Pawlicka

Received: 15 November 2013 / Accepted: 15 April 2014 / Published online: 1 May 2014

Abstract Polysaccharide- and gelatin-based bioblends and polyblends were synthesized and characterized by complex impedance spectroscopy, proton nuclear magnetic resonance (NMR) and electron paramagnetic resonance (EPR). Higher ionic conductivities of 7.9×10^{-5} S/cm at room temperature and 2.5×10^{-3} S/cm at 80 °C were obtained for the agar-chitosan polyblends. For all samples, the activation energies, calculated from the Arrhenius plot of ionic conductivity and from the onset of NMR line narrowing, are in the range 0.30–0.86 and 0.38–0.57 eV, respectively. The glass transition temperatures (T_g^{NMR}) varied from 200 to 215 K, depending on the sample composition. The temperature dependence of the ^1H spin–lattice relaxation revealed two distinct proton dynamics. The EPR spectra are characteristic of Cu^2 ions in tetragonally distorted octahedral sites. Quantitative analysis of the EPR spin Hamiltonian $g_{||}$ and $A_{||}$ parameters revealed copper ions complexed by nitrogens and oxygens in the samples containing chitosan or gelatin and only by oxygens in agar-based ones. The in-plane π bonding is less covalent for the gelatin and chitosan blends. Results suggest that natural bioblends and polyblends are interesting systems to be used in materials science engineering.

Keywords Natural macromolecules · Bioblends · Impedance · Solid state NMR · EPR

R. I. Mattos · C. E. Tambelli
FZEA, Universidade de São Paulo, Pirassununga, SP 13635-900, Brazil

R. I. Mattos · E. Raphael · A. Pawlicka (✉)
IQSC, Universidade de São Paulo, São Carlos, SP 13566-590, Brazil
e-mail: agnieszka@iqsc.usp.br

E. Raphael
DCNAT, Universidade Federal de São João Del Rei, PO Box 110, São João Del Rei, MG 36301-160, Brazil

I. D. A. Silva · C. J. Magon · J. P. Donoso
IFSC, Universidade de São Paulo, PO Box 369, São Carlos, SP 13560-970, Brazil

Introduction

Blends are defined as one-phase miscible or two-phase partially miscible or immiscible systems (Chanda and Roy 2006). From the historical point of view, these materials have always been known and used; however, only in the past century did they started to be investigated with technological interest. Polymer blends, also known as polyblends, are produced by a physical mixture of two or more polymers or copolymers and present as a new polymeric material with improved properties compared to those of its constituents (Chanda and Roy 2006). Recently, polyblends obtained from natural polymers have gained greater interest because of their advantages in relation to petroleum-based polyblends (Yu et al. 2006). Natural macromolecules are easily extracted from fast-

growing plants or crustaceans, but can also be obtained from bacterial synthesis, resulting in almost pure polymers (Cremona et al. 2008). Polysaccharides and gelatin are also relatively cheap, biodegradable and biocompatible with human tissue, which is an important property for biomedical materials development (Ciardelli and Chiono 2006; Rinaudo 2006). Because chitosan-gelatin polyblends have antimicrobial properties (Gomez-Estaca et al. 2011), they are being applied for cartilage defect regeneration (Guo et al. 2006) and scaffolding for guided tissue regeneration (Huang et al. 2005; Hong et al. 2009). Moreover, it has been suggested that these materials can enhance nerve cell attachment and make the mechanical properties of scaffolds more similar to those of nerve tissues (Ciardelli and Chiono 2006; Cheng et al. 2003). It has been remarked that the nerve regeneration is due to the presence of polysaccharides and good cell adhesion properties of the protein phase (Ciardelli and Chiono 2006).

Another method to obtain blends and alter the physical–chemical properties of the polymeric materials is by addition of plasticizers (Pawlicka et al. 2008). The influence of the plasticizer on the thermal, mechanical and permeation properties of the chitosan-gelatin-water or polyol edible blends has been described (Hong et al. 2009). A decrease in the mechanical strength, melting and glass transition temperatures and increase in the gas/water permeation rates proportional to the total plasticizer content in the samples have been noted (Hong et al. 2009). Although several reports on chitosan-gelatin polyblends have already been published, just a few reports related to the preparation and characterization of chitosan-agar polyblends can be found (El-Hefian et al. 2010).

Most of the bio-macromolecules are polyelectrolyte (Yalpani 1988) and can dissolve inorganic salts or acids (Pawlicka et al. 2008; Raphael et al. 2010), making possible the use ionic conductivity and solid-state NMR measurements to study the ionic and polymer chain dynamics (Chung et al. 1998; Bohmer et al. 2007; Walderhaug et al. 2010). The temperature dependence of the NMR line shapes and spin–lattice relaxation times provides an effective and selective probe of the spin dynamics on the Hz to MHz frequency scale, supplying valuable information on the molecular motions that modulate the magnetic dipolar and electric quadrupolar interactions (Bohmer et al. 2007; Eckert 1992). With the EPR measurements, it is possible to investigate the local environment and the coordination geometry of the Cu^{2+} ion in the biomembranes (Pawlicka et al. 2013). Transition metals, such as Cu^{2+}, Fe^{3+} and Mn^{2+}, are widely studied by EPR spectroscopy because of their importance in biological and catalytic systems (Pilbrow 1990; Boobalan and Rao 2010; Peisach and Blumberg 1974). In particular, the hyperfine structure of the Cu^{2+} ion, with an effective electron spin of 1/2 and a nuclear spin of 3/2, is an interesting and useful EPR probe. Since Cu^{2+} EPR spectra are very sensitive to symmetry and strengths of the ligand field in the immediate environment of the paramagnetic ion, the EPR data combined with optical absorption spectroscopy are used to obtain information about the nature of the ground state of Cu^{2+} ions and the nature of the bonding between the copper 3d orbital and the ligand orbitals. Finally, the interest in the complexation behavior of the Cu^{2+} ion comes from its importance regarding the biological activity of the membranes (Singh et al. 2008).

Aiming to progress in the understanding of the natural macromolecule materials for medical and engineering applications, the present article provides the results of complex impedance spectroscopy, ^{1}H NMR and EPR studies of the agar and chitosan blends and polyblends. The work focuses on the proton mobility and coordination geometry of copper ions in these biomaterials and is a continuation of recently reported conductivity and magnetic resonance investigations on chitosan-based biomembranes (Pawlicka et al. 2013).

Experimental

All membranes, i.e., chitosan, gelatin and agar blends and chitosan-agar and chitosan-gelatin polyblends, were obtained by the solution casting method. The solutions were poured onto petri plates and allowed to form membranes that were dried at 50 °C for 48 h and stored in a desiccator. The formulations of chitosan, gelatin and agar blends with higher conductivity were used to obtain the chitosan-agar and chitosan-gelatin polyblends.

Chitosan blends were prepared by dispersing 0.55 g of chitosan (Aldrich, no. 448877; average molecular mass of 3–6 × 10^4; viscosity of 200–800 cps with

1 % CH_3COOH and measured deacetylation degree of 70 %) in 55 ml of acetic acid solution (excess of 21.7 times to amine groups in chitosan), previously prepared with concentrations of 5 % (0.87 mol/l) in Millipore Milli-Q® water with resistivity of 18 $m\Omega^{-1}cm^{-1}$ at 25 °C. For homogeneous gel formation, this solution was left under magnetic stirring for 24 h and vacuum filtered. Then, 0.8 g of glycerol was added as plasticizer, and the mixture was stirred for a few minutes to obtain homogeneous solution.

Gelatin blends were prepared by dispersing 2.0 g of commercial uncolored gelatin (Oetker®) in 15 ml of Millipore Milli-Q® water and heating under magnetic stirring up to 50 °C for complete dissolution. Then, 1.25 g of glycerol (Synth) as plasticizer, 0.25 g of formaldehyde (36.5–38.0 %; Synth) as cross-linking agent and 1.25 g of acetic acid (99.7 %; Quemis) were added and stirred for a few minutes to obtain homogeneous solution.

Agar blends were prepared by dispersing 0.5 g of agar (Sigma-Aldrich) in 25 ml of Milli-Q® water and heating under magnetic stirring up to 100 °C for complete dissolution. Then 0.5 g of glycerol as plasticizer, 0.5 g of formaldehyde as cross-linking agent and 1.5 g of acetic acid were added to the solution and stirred for a few minutes to obtain homogeneous solution.

Chitosan-gelatin and chitosan-agar polyblends were obtained by mixing and stirring the respective solutions at 50 °C for 20 min.

Complex impedance spectroscopy measurements were performed on membranes with the shape of discs sandwiched between two stainless-steel electrodes and placed under reduced pressure in a hermetically closed Teflon holder. Impedance data were collected with a Solartron model 1260 using an AC potential of 50 mV in the temperature range of 298 K (25 °C)–358 K (85 °C) and frequency range of 10 Hz–1 MHz.

The UV-Vis-NIR optical spectra of the samples were recorded with an Agilent Spectrophotometer Instrument 8453 between 500 and 1,000 nm.

Proton ^1H linewidth and spin–lattice relaxation time measurements were carried out from 150 to 380 K on a home-built NMR spectrometer equipped with a Tecmag NMR kit, operating at 36 MHz. Spectrum linewidth was determined using a single pulse sequence, with a typical non-selective $\pi/2$ pulse length of about 2 μs. The spin–lattice relaxation time was determined with the standard saturation-recovery pulse sequence, the magnetization recoveries toward equilibrium being found to be exponential throughout the entire temperature range.

Continuous-wave electron paramagnetic resonance (CW-EPR) spectra were obtained at 15 K on a BrukerElexsys E580 spectrometer operating at 9.5 GHz (X-band), with the temperature controlled by a continuous flow liquid helium Oxford cryogenic system. The EPR experiments were carried out in samples doped with copper perchlorate (0.001 mol/l).

Results and discussion

To analyze the ionic conductivity properties of the bioblends and biopolyblends, complex impedance spectroscopy was measured as a function of the temperature. Figure 1a shows the appearance of an impedance semicircle at high frequencies, followed by a spike-like response at low frequencies in the Nyquist plot of agar, chitosan blends and chitosan–agar and chitosan–gelatin polyblends at room temperature. The Nyquist plot of gelatin-based samples is shown in the work of Vieira et al. (2007). According to the literature, such a semicircle-like impedance response can be simulated by an equivalent circuit consisting, ideally, of a parallel resistance-capacitance (R-C) arrangement. In our case, the experimental data were fitted with an equivalent circuit model using Zview2 software. In the used model (inset of Fig. 1a), R1 is the membrane-electrode charge transfer resistance, R2 is the electrolyte resistance in parallel with the constant phase element (CPE), which is an imperfect capacitor, and W is the Warburg element responsible for the diffusional control of the system. As can be observed in this figure and similarly to Yu et al. (2007), good agreement between both experimental and impedance fitting was obtained.

The impedance measurements were then used to obtain membranes' bulk resistance (R_b) from the intercept of the semicircle with the Nyquist plot real axis. Then, the dc ionic conductivity was deduced from the R_b values by employing the formula $\sigma = l/R_bA$, where l is the thickness of the membrane, and A is the contact area between the sample and the electrode. Figure 1b shows the behavior of the conductivity (σ) as a function of the reciprocal temperature for the chitosan, gelatin and agar blends and the chitosan-agar and chitosan-gelatin polyblends

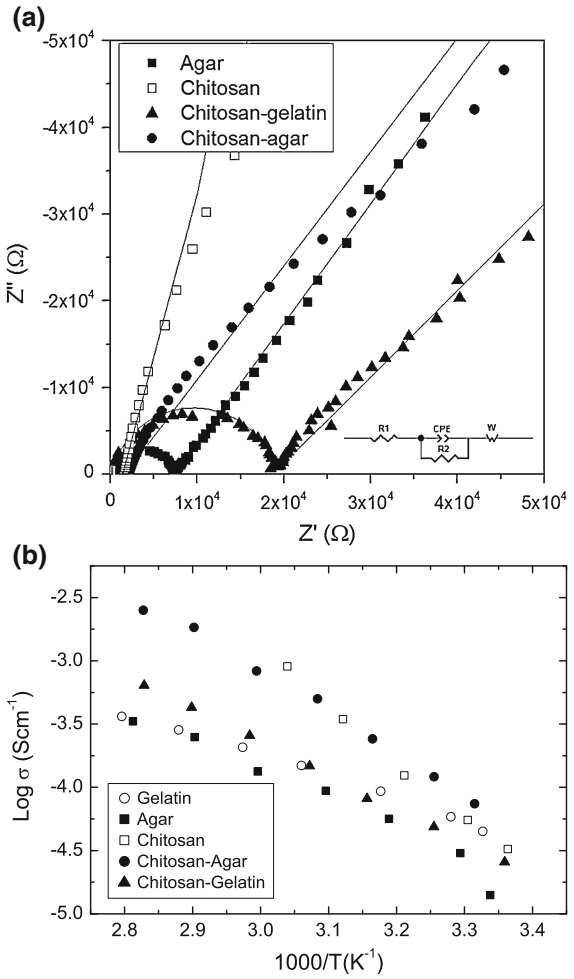

Fig. 1 Nyquist plot of agar (*filled square*) and chitosan blend (*open square*), chitosan–gelatin (*filled triangle*) and chitosan–agar polyblends (*filled circle*) with equivalent circuit model (*inset*). Fittings are in straight lines (**a**). Temperature dependence of the logarithm of the ionic conductivity for the bioblends and polyblends (**b**)

investigated. As can be observed in this figure, the polyblends display a significant increase in conductivity values when compared to the results obtained for the gelatin and agar blends separately. The increase in the ionic conductivity as a function of temperature is mainly due to the blend formulation and temperature. Since the glass transition temperature of the system is very low, the polymeric chains can move easily and create the free volume and/or help in ion transportation. The ionic conductivity of natural polymer-based samples can be explained by two models, i.e., the Grotthuss model, where the ion movement is due to

Table 1 Values of the ionic conductivity and activation energy for the bioblends and polyblends

Sample	Conductivity room temperature (S/cm)	E_a (kJ/mol)	E_a (eV)
Gelatin	4.5×10^{-5}	28.3	0.30
Chitosan	3.2×10^{-5}	82.5	0.86
Agar	2.0×10^{-5}	43.3	0.45
Chitosan-agar	5.4×10^{-5}	56.1	0.58
Chitosan-gelatin	2.3×10^{-5}	53.2	0.55

ion displacement between cation-heteroatom coordinations (Wright 1975), and the vehicular or VTF model (Kreuer 1997), where the ions move with the chain movement because of the free volume environment (Pawlicka et al. 2013; Mattos et al. 2010). The ionic conductivity values of 5.4 and 2.3×10^{-5} S/cm at 300 K of the chitosan-agar and chitosan-gelatin polyblend, respectively, are in good agreement with those reported for the samples of plasticized chitosan–poly(ethylene oxide) (PEO) and chitosan-poly(vinyl alcohol) (PVA) polyblends prepared with ammonium nitrate (Kadir et al. 2009, 2010; Shukur et al. 2013). Moreover, it can be stated that the ionic conductivity value of the chitosan-agar polyblend at 300 K is about twice the value obtained for the chitosan–gelatin sample at the same temperature. This difference can be due to the acetic acid content in the sample being 59 % for the chitosan-agar and 35 % for the chitosan-gelatin sample. Figure 1b also reveals an increase in the conductivity values with temperature. At 353 K the values are $2.5 \times 10^{-3}$and 6.4×10^{-4} S/cm for the chitosan-agar and chitosan-gelatin polyblend, respectively. Again, these values are higher when compared with the values of 3.6 and 3.3×10^{-4} S/cm found in the gelatin and agar blend samples at the same temperature. Probably, the addition of chitosan plays an important role in the significant improvement in conductivity.

The ionic conductivity as a function of temperature reveals an Arrhenius behavior with activation energy values (E_a) of 53.2 kJ/mol (0.55 eV) and 56.1 kJ/mol (0.58 eV) for the chitosan-gelatin and chitosan-agar polyblend membranes, respectively (Table 1). Usually the lower E_a, the higher σ is; thus, the polymer environment facilitates the ion movement, which results in higher ionic conductivity. In the present work, it should be noted that the activation energies of the polyblends are higher than those obtained for the

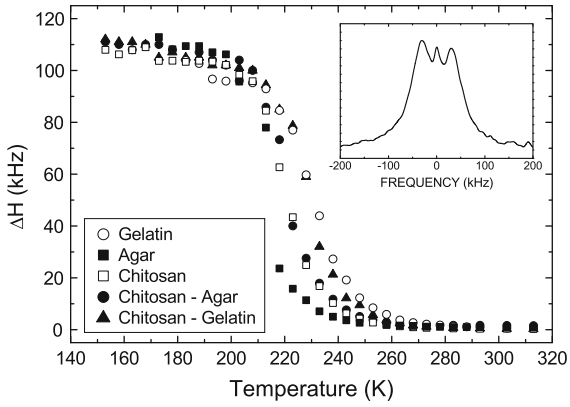

Fig. 2 Temperature dependence of the ^{1}H NMR linewidth of the bioblends and polyblends. The *inset* shows the ^{1}H NMR spectra at 153 K for the chitosan-gelatin polyblend

samples based on gelatin and agar blends that showed the values of 28.3 (0.3 eV) and 43.3 kJ/mol (0.45 eV), respectively. These E_a values are smaller than the value of 82.5 J/mol (0.86 eV) for the chitosan blend doped with acetic acid shown in Table 1, as well as in other works (Pawlicka et al. 2013; Donoso et al. 2007). However, because of their different acid concentrations, it is difficult to establish a quantitative comparison among the conductivity values of these biosamples.

Aiming to investigate the ionic and polymer dynamics of the obtained biomembrane samples, solid-state NMR was used (Chung et al. 1998; Bohmer et al. 2007; Walderhaug et al. 2010). Figure 2 shows the temperature dependence of the ^{1}H NMR linewidth for the natural polymer-based membranes. The inset in Fig. 2 shows the ^{1}H static NMR spectrum recorded at 153 K for the chitosan-gelatin polyblend. As can be observed in this figure, the spectrum exhibits the same line pattern of those observed previously for gelatin and chitosan blends at low temperature, where a narrow central resonance line, flanked by a pair of peaks attributed to a Pake doublet, is observed (Pawlicka et al. 2011, 2013). The central line can be assigned to the superposition of the ^{1}H signals belonging to the OH and CH groups and the doublet belong to the intermolecular interactions between the protons of molecular groups, such as CH_2 and NH_2. The CH_3 groups contribute to the triplet structure of the spectrum (Pawlicka et al. 2011, 2013). Analysis of the Fig. 2 inset, which is representative to all samples, clearly shows a large broadening caused by the dipole-

Table 2 NMR parameters obtained from ^{1}H NMR linewidth for the bioblends and polyblends

Sample	ΔH (kHz)	T_g^{NMR} (K)	E_a(kJ/mol)	E_a (eV)
Gelatin	104	215 ± 3	41.5	0.43
Chitosan	108	205 ± 3	47.3	0.49
Agar	113	200 ± 3	36.7	0.38
Chitosan-agar	108	201 ± 3	46.3	0.48
Chitosan-gelatin	107	212 ± 3	55.0	0.57

ΔH is the low temperature linewidth; T_g^{NMR} is the glass temperature transition determinant from the onset of NMR line narrowing; E_a is the activation energy for the line-narrowing process

dipole intra- and intermolecular interactions between protons of different molecular groups of the gelatin, agar, chitosan and glycerol (Pawlicka et al. 2011, 2013).

The low temperature dependence of the ^{1}H NMR linewidth, shown in Fig. 2, reveals that the spectra are essentially unchanged up to approximately 200 K for all samples, meaning that the proton mobility in these membranes is restricted at low temperatures. However, above 200 K, the central and broad lines begin to narrow because of the motional narrowing caused by the increase in proton mobility. The final residual linewidth observed at higher temperatures is only a small fraction of the initial low-temperature *rigid lattice* value. In ionically conducting samples, the onset of the ^{1}H line narrowing is associated with the calorimetric glass transition temperature (T_g^{NMR}) (Bohmer et al. 2007; Pawlicka et al. 2013). Therefore, from the data in Fig. 2, it is possible to estimate the T_g^{NMR} values that range from 200 to 215 K, depending on the sample (Table 2). The detailed analysis of the polyblend values also reveal that in the chitosan-agar sample, the motional narrowing starts at about 200 K, which is 12 K below the onset temperature observed in the chitosan-gelatin sample. This difference can be explained in terms of proton mobility that increases at lower temperatures for the chitosan-agar than for the chitosan-gelatin polyblend (Ogihara et al. 2004). This result is in agreement with the difference observed between the ionic conductivity of both polyblends showed in Fig. 1b.

The activation energy for the NMR line-narrowing processes was evaluated by assuming a thermally activated process following an Arrhenius temperature dependence for the correlation times associated with

the proton motion (Wilkening et al. 2002; Lopes et al. 2003). From the analysis of the line-narrowing data in Fig. 2, it was possible to calculate the activation energies of 46.3 kJ/mol (0.48 eV) for the chitosan-agar and 55 kJ/mol (0.57 eV) for the chitosan-gelatin polymer blends. It should be noted that the activation energies obtained from conductivity measurements may not coincide with those determined from NMR measurements because these techniques do not probe the same dynamic processes. Since the correlation function of the impedance spectroscopy is sensitive to fast-charged species motion, the conductivity measurements probe long-range ion migration. The NMR line-narrowing process, which takes place when the rate of the fluctuations of the local dipolar fields is of the order of the low temperature *rigid lattice* linewidth, is dominated by low-frequency (kHz) fluctuations in the local magnetic field on the nuclei. In contrast, the correlation function governing NMR spin–lattice relaxation samples short-range motions of the probe nuclei in the Larmor frequency range (MHz) (Bohmer et al. 2007; Winter et al. 1997).

Figure 3 shows the temperature dependence of the ^{1}H NMR spin–lattice relaxation rate (T_1^{-1}) of chitosan-gelatin, chitosan-agar polyblend, and agar, chitosan and gelatin blend membranes. The main relaxation process observed in this figure is of dipolar origin and is due to the thermal motion of protons, which modulates the ^{1}H–^{1}H dipolar interactions. It is interesting to note that the ^{1}H relaxation times, measured at the same Larmor frequency in the proton-conducting membranes studied here, are of the same order of magnitude, where T_1 varies from about 30 ms to 1.0 s in the temperature range investigated. The temperature dependence of the relaxation rate T_1^{-1} is usually analyzed using the simple Bloembergen, Purcell and Pound (BPP) model (Bohmer et al. 2007; Pawlicka et al. 2013). The spin–lattice relaxation rate is parameterized by the NMR Larmor frequency (ω_o), by a constant that depends on the spin interaction responsible for the relaxation (C) and by the correlation time (τ_c) of the molecular motion modulating the nuclear spin interactions. Arrhenius temperature dependence for τ_c is often assumed for the correlation time, $\tau_c = \tau_o\, exp(E_a/k_B T)$, where k_B is the Boltzmann constant, E_a is the activation energy, and τ_o is the pre-exponential factor. Inspection of Fig. 3 shows that the relaxation curves have similar shapes and display a single relaxation rate maximum, indicating that the relaxation mechanism is the same for all analyzed samples. Furthermore, an asymmetric shape around the relaxation rate maximum is also observed in all plots. This asymmetry was interpreted assuming the existence of two distinct proton dynamics, one associated with the protons of the acetic acid and another one caused by protons in different environments (Mattos et al. 2010). Therefore, the experimental ^{1}H relaxation rate for both polyblend samples was deconvoluted into two BPP theoretical spin–lattice relaxation curves, shown in Fig. 4 (Pawlicka et al.

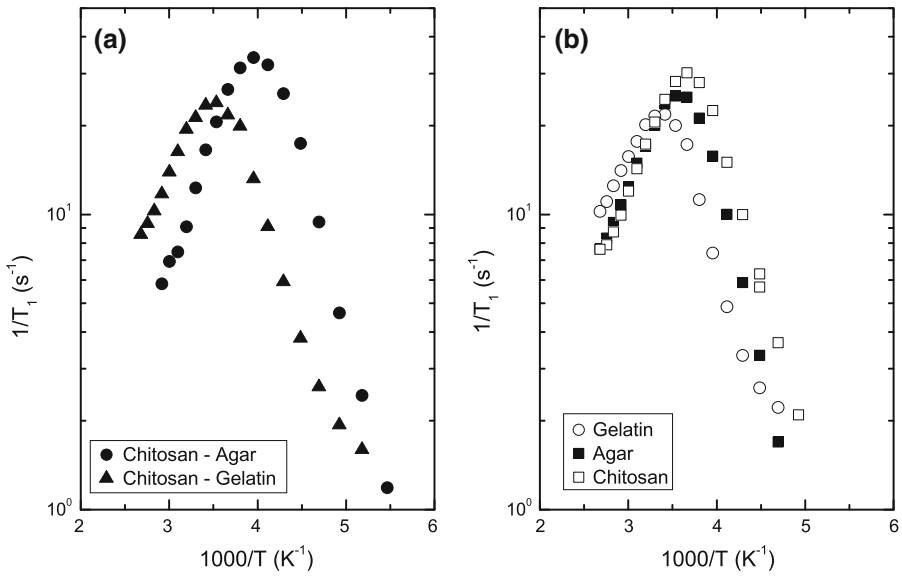

Fig. 3 Temperature dependence of the ^{1}H spin–lattice relaxation rates ($1/T_1$) for the chitosan-agar and chitosan-gelatin polyblends (**a**) and for the gelatin, agar and chitosan blends (**b**)

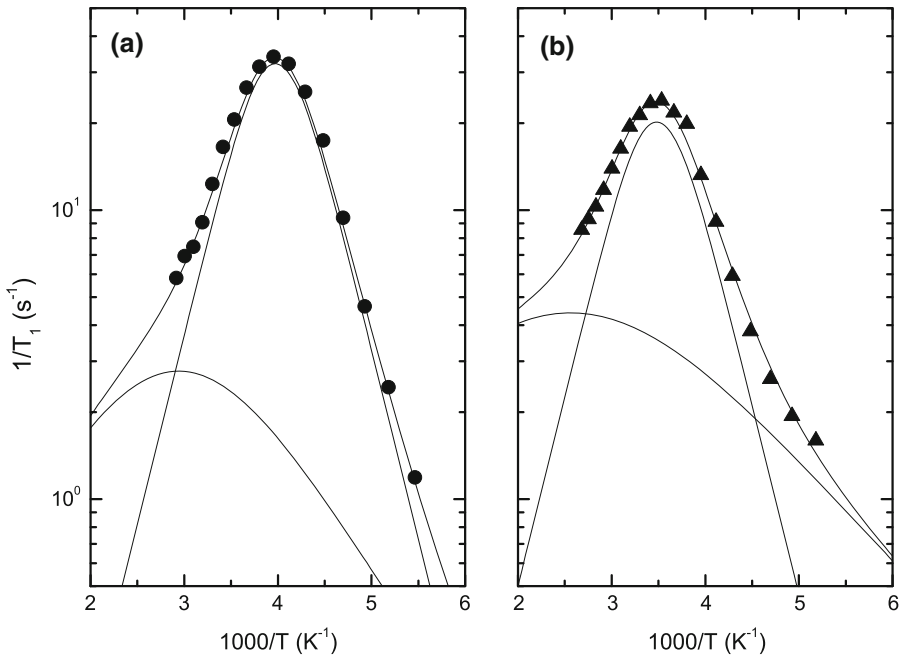

Fig. 4 Temperature dependence of the ^{1}H spin–lattice relaxation rates (T_1^{-1}) for the chitosan-agar (**a**) and chitosan-gelatin polyblend (**b**). The *solid lines* correspond to the BPP fitting

2013; Mattos et al. 2010). As can be seen in Fig. 4, the simulated curves closely reproduce the temperature dependence of the experimental data.

The dynamic parameters such as E_a and τ_o obtained from the BPP analysis of the ^{1}H NMR relaxation data for the studied samples are summarized in Table 3. It should be remembered that the activation energies determined from conductivity measurements for the blend and polyblend samples were higher than those obtained from NMR data (Tables 1, 2). As mentioned above, this is likely to be a result of the different time scales of the NMR spin relaxation compared with conductivity measurements.

The BPP model predicts the presence of a spin–lattice relaxation rate maximum at a given temperature, T_{max}, at which the condition $\omega_o\tau_c \approx 0.62$ is satisfied. Furthermore, the value of the relaxation rate maximum $(T_1^{-1})_{max}$ depends upon the strength of the spin interaction responsible for the relaxation (the constant C). In the case of the ^{1}H resonance in proton-conducting membranes, this constant C is related to the mean-square amplitude of the fluctuating proton-proton dipole-dipole interactions. Therefore, the slight differences in the value of $(T_1^{-1})_{max}$ observed in Fig. 3 reflect modifications in the interaction distance or in the nature of the interaction itself such as, for example, homonuclear and heteronuclear interactions (Pawlicka et al. 2011; Ng et al. 1998).

Providing that the activation energies of the studied samples do not differ very much, one can compare the relative mobility of the protons in different samples by comparing the temperature position of the ^{1}H relaxation rate maxima (Ng et al. 1998). The T_1^{-1} maximum occurring at lower temperatures in the chitosan-agar polymer blend, when compared the chitosan-gelatin one, is an indication of higher proton mobility. The shift in T_{max} toward lower temperature is in agreement with the low T_g^{NMR} observed for this sample (Fig. 3). Moreover, this chitosan-agar polyblend exhibits the highest room temperature conductivity of 5.4×10^{-5} S/cm and the lowest room temperature correlation time of 4.0×10^{-10} s when compared with other samples (Tables 1, 3). It should be noted that the conductivities and the NMR results in these proton-conducting membranes seem not to be directly related with the acetic acid and/or the glycerol content in the sample. The relationship between conductivity and acid (or salt) concentration in conducting membranes is a complex matter because of several factors, such as the charge-carrier concentration, plasticizer nature and charge-carrier mobility, which contribute to the conductivity (Chung et al. 1998; Mattos et al. 2010; Ng et al. 1998).

Aiming to analyze the local environment and the coordination geometry of copper cations in the bioblends and polyblends, EPR measurements were

Table 3 NMR parameters obtained from ^{1}H NMR spin–lattice relaxation rates for the bioblends and polyblends

Sample	Process	T_{max} (K)	E_a (eV)	τ_o (s)	τ_c (300 K) (s)	$(T_1^{-1})_{max}$ (s^{-1})
Chitosan	1	270	0.25	2.9×10^{-14}	4.6×10^{-10}	30
Gelatin	1	293	0.35	0.28×10^{-14}	21.2×10^{-10}	22
	2	–	0.12	5.0×10^{-11}	–	–
Agar	1	280	0.30	1.0×10^{-14}	11.0×10^{-10}	25
	2	–	0.14	2.5×10^{-11}	–	–
Chitosan-agar	1	253	0.26	1.7×10^{-14}	4.0×10^{-10}	33
	2	–	0.10	9.0×10^{-11}	–	–
Chitosan-gelatin	1	283	0.26	7.5×10^{-14}	17.0×10^{-10}	23
	2	–	0.08	34.0×10^{-11}	–	–

T_{max} is the temperature of the relaxation rate maximum; $T_1^{-1}{}_{max}$ is the relaxation rate maximum; E_a is the activation energy for the motion causing the proton relaxation; τ_o is the pre-exponential factor of the correlation time, and τ_c is the room temperature correlation time

performed. Copper perchlorate was chosen because of the paramagnetic properties of the Cu^{2+} ion, and the stability of the samples was confirmed by thermogravimetry (TGA) analysis (not shown here) revealing about 5 % weight loss up to 150 °C. Figure 5 shows the EPR spectra of biomembranes containing Cu^{2+} at 50 K. Spectra A and B in Fig. 5 are similar to those previously reported for gelatin-based membranes (Mattos et al. 2010) and for chitosan biomembranes doped with $Cu(ClO_4)_2$ (Pawlicka et al. 2013). The overall shapes of the observed spectra in Fig. 5 are typical of paramagnetic Cu^{2+} ions in axially distorted sites, but some significant differences can be observed. The low field part of the spectra in Fig. 5, i.e., around 3,000 G and corresponding to $g_{||}$, shows a set of four evenly spaced copper hyperfine lines, whereas in the high field part of the spectra, i.e., around 3,300 G and corresponding to $g_{\perp}$, the hyperfine satellites are not resolved, and a single line is observed. These hyperfine structures result from the dipole-dipole interaction between the magnetic moment of the ^{63}Cu and ^{65}Cu nuclei (nuclear spin $I = 3/2$) and the electronic moment of the paramagnetic Cu^{2+} ion ($3d^9$ electronic configuration, spin S = 1/2) (Giua et al. 1996). No additional features associated with the superhyperfine interaction between the Cu^{2+} electronic spin with neighboring ^{14}N nuclei (spin $I = 1$) are observed in the measured EPR spectra.

The Cu^{2+} EPR spectrum is usually described by an axial spin Hamiltonian, H, that includes the hyperfine interaction,

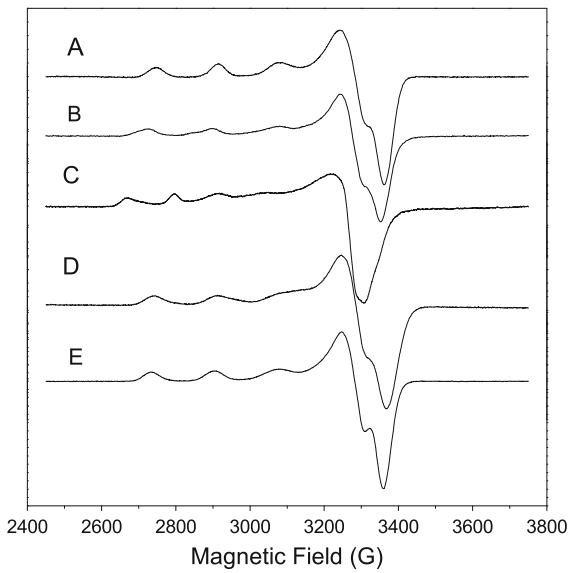

Fig. 5 X-band EPR spectra measured at 15 K of the chitosan (*A*), gelatin (*B*), agar blends (*C*) and chitosan-gelatin (*D*) and chitosan–agar polyblend (*E*)

$$H = g_{||}\beta H_z S_z + g_{\perp}\beta(H_x S_x + H_y S_y) + A_{||} I_z S_z + A_{\perp}(I_x S_x + I_y S_y) \quad (1)$$

where z is the tetragonal symmetry axis; H_x, H_y and H_z are the components of the static magnetic field; S and I are the electron and the nuclear spin operators; $g_{||}$ and $g_{\perp}$ are the parallel and perpendicular components of the anisotropic g tensor; $A_{||}$ and $A_{\perp}$ are the parallel and perpendicular hyperfine components of the hyperfine tensor A, and β is the Bohr magneton (Pawlicka et al.

Table 4 Summary of Cu^{2+} spin Hamiltonian and bonding parameters for the bioblends and polyblends

Sample	Area (%)	$g_{\|}$	$g_{\perp}$	$A_{\|} \times 10^{-4}$ cm^{-1}	α^2	β^2	$\Delta E_{yx} \times 10^4$ cm^{-1}
Chitosan		2.261	2.056	170	0.80	0.62	1.28
Gelatin	39	2.299	2.056	191	0.89	0.67	1.33
	61	2.268	2.069	207	0.91	0.59	
Agar	62	2.366	2.068	137	0.82	0.81	1.20
	38	2.381	2.063	117	0.77	0.88	
Chitosan-gelatin	60	2.263	2.060	173	0.81	0.65	1.33
	40	2.235	2.065	183	0.81	0.58	
Chitosan-agar		2.265	2.054	173	0.81	0.64	1.31

2013; Pilbrow 1990). The first two terms in Eq. 1 represent the interaction between the electronic spin and the magnetic field and the third and fourth terms the coupling between the electronic and nuclear spins.

The experimental Cu^{2+} EPR spectra in Fig. 5 were analyzed by numerical simulation of the spin Hamiltonian (Eq. 1) by using the EasySpin package in the Matlab environment (Stoll and Schweiger 2006) for a 1/2 spin with an anisotropic *g*-tensor and hyperfine coupling. As previously reported, the observed line shape of the gelatin blend samples (Fig. 5B) (Pawlicka et al. 2011) is a superposition of two spectral components, corresponding to two different copper species. In the case of the agar blend sample (Fig. 5C), also two components were necessary to simulate the experimental EPR spectrum. The spin Hamiltonian parameters, deduced from the simulated spectra, are collected in Table 4. The error in the EPR parameters obtained from the fitting procedure was estimated to be ±2 G for $A_{\|}$ and ±0.001 for $g_{\|}$ and $g_{\perp}$. It should be noted that the spin-Hamiltonian parameters (Table 4) are consistent with those previously reported for copper in gelatin gel electrolytes (Pawlicka et al. 2011) and for copper complexes stabilized with chitosan (Kramareva et al. 2003; Justi et al. 2004).

Figure 6 shows the experimental (continuous line) and simulated spectra (dotted line) of two representative spectra: chitosan-gelatin and chitosan-agar polyblends. The simulated spectra closely reproduce the position and intensities of the prominent features of all spectra.

Detailed quantitative information on the coordination environment of Cu^{2+} ions in the biomembranes can be obtained by analyzing the EPR spin Hamiltonian parameters. The parallel components of the tensors ($g_{\|}$ and $A_{\|}$) are sensitive to changes in geometry and ligand binding and therefore can be used to interpret experimental EPR data (Pilbrow 1990; Carl and Larsen 2000). The empirical model originally suggested by Blumberg and Peisach correlates the Cu^{2+} pair of parameters ($g_{\|}$ and $A_{\|}$) and has been applied extensively to proteins and copper-exchanged zeolites (Peisach and Blumberg 1974; Carl and Larsen 2000). When the EPR parameters are plotted in a $g_{\|}$ versus $A_{\|}$ graph, a correlation can be found between these values and the nature of the equatorial coordinating atoms. Figure 7 shows a so-called Peisach-Blumberg plot for biomembranes using the $g_{\|}$ and $A_{\|}$ from Table 4. In the construction of this graph, no distinction was made between the $g_{\|}$ and $A_{\|}$ values of the different copper species of the same membrane. Since the goal was to analyze the nature of the coordinating atoms exclusively, the same symbols were used in Fig. 7 for the different Cu^{2+} species of

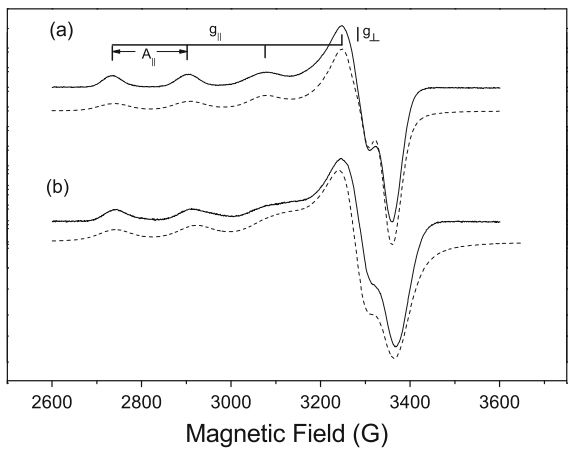

Fig. 6 Experimental and simulated EPR spectra of the chitosan-agar (*a*) and chitosan-gelatin polyblends (*b*)

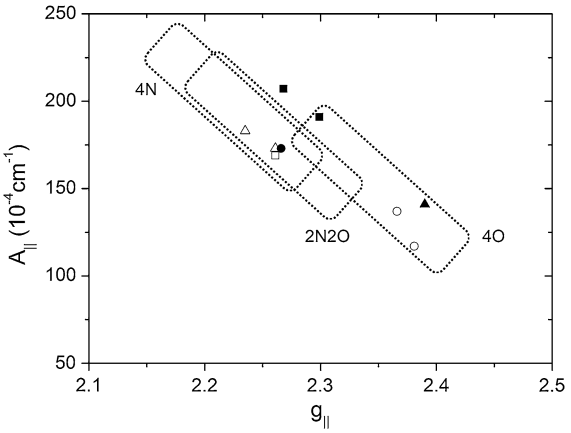

Fig. 7 Correlation plot of $g_{\|}$ and $A_{\|}$ of the gelatin (*filled square*), agar (*open circle*), chitosan blend (*open square*), chitosan-gelatin (*open triangle*) and chitosan-agar polyblends (*filled circle*), and PEO_{40}:$Cu(ClO_4)_2$ (*filled triangle*)

the same membrane. The values of $g_{\|} = 2.39$ and $A_{\|} = 141 \times 10^{-4}$ cm^{-1} of the PEO doped with copper perchlorate (PEO:$Cu(ClO_4)_2$) are also included in Fig. 7 (Donoso et al. 1995). The dashed lines in Fig. 7 show, with a substantial overlap, the relative position for the Cu^{2+} ion with four oxygen ligands (4O), two nitrogens and two oxygen ligands (2N2O) and four nitrogens (4 N). As expected, the $g_{\|}$ and $A_{\|}$ parameters of the agar blend, as well as those of the PEO:$Cu(ClO_4)_2$, fall within the region corresponding to the coordination of Cu^{2+} ions only by oxygens, whereas those of the gelatin and the chitosan blends fall in the region corresponding to cooper ions coordinated to nitrogen and oxygen atoms (Fig. 7). The involvement of nitrogen atoms in the copper complexation of the gelatin-based sample was verified in our previous work by electron spin echo envelope modulation (ESEEM) (Mattos et al. 2010). Perhaps the most important result in Fig. 7 is the observation that the $g_{\|}$ and $A_{\|}$ parameters for both chitosan-based polyblends fall in the region where oxygen and nitrogen are coordinating the Cu^{2+}. Thus, these results highlight the importance of the chitosan in the complexation of copper ions in the samples. In particular, for the chitosan-agar polymer blend, the result in Fig. 7 reflects the reluctance of the agar polysaccharide to coordinate the copper ion in this membrane.

As mentioned above, EPR spectroscopy can provide valuable information concerning the local environment of paramagnetic ions. EPR spectra with "axial symmetry" (e.g., Cu^{2+} in the present study), i.e., with one principal axis of symmetry, conventionally the z-axis, exhibit two g values, labeled $g_{\|}$ parallel to the z-axis or $g_{\perp}$ perpendicular to the z-axis, i.e., in the x-y plane. The relative value of these two parameters in relation to the "free electron g-factor," $g_e = 2.0023$, indicates the predominance of the d_{z2} or the d_{x2-y2} orbital in the ground state. For example, in the case of $g_{\|} > g_{\perp} > g_e$, the geometry corresponds to a tetragonal elongated configuration, with d_{x2-y2} being the ground state. For $g_{\perp} > g_{\|} \geq g_e$, tetragonal compressed configuration and trigonal bipyramidal geometries are expected with d_{z2} being the ground state (Pilbrow 1990; Hathaway and Billing 1970; Stosser et al. 1999; Vedeanu et al. 2012). Analyzing the EPR results resumed in Table 4, it is seen that $g_{\|} > g_{\perp} > g_e$ in all the samples. This is consistent with Cu^{2+} ions being located in axial elongated symmetry (square planar, square pyramidal and distorted octahedral geometries). From the g values and the EPR spectra, it can be concluded that the ground state of Cu^{2+} is the d_{x2-y2} orbital, i.e., the $^2B_{1g}$ state (Pilbrow 1990). The parameter G, which is a measure of the exchange interaction between the copper centers in the complex, can be calculated by using the expression appropriate for axial EPR spectra, $G = (g_{\|}-g_e)/(g_{\perp}-g_e)$ (Procter et al. 1968). If $G > 4.0$, the exchange interaction is considered negligible; if it is <4.0, considerable exchange coupling is present in the complex. Since the G values calculated for the biomembranes are within the range of 3.9–5.5, exchange coupling effects are not significant, and the observed g values are considered to reflect the local Cu^{2+} ion environment.

The nature of metal ligand bonding can be analyzed using coefficients calculated from the EPR spin Hamiltonian parameters and the optical absorption spectra of the Cu^{2+} doped samples shown in Fig. 8. According to the molecular orbital (MO) theory approach (Pilbrow 1990; Kivelson and Neiman 1961), the bonding parameters are described in terms of the covalency parameters α^2 and β^2. The parameter α^2 describes the covalency of the in-plane σ bonding between a copper 3d orbital and ligand orbitals, quantifying the delocalized electronic density on the ligand atoms. Its value decreases with increasing covalency to a minimum value of $\alpha^2 = 0.5$ for a completely covalent copper-ligand bond up to a maximum value of $\alpha^2 = 1.0$ for a completely ionic bond. Within the framework of the MO model

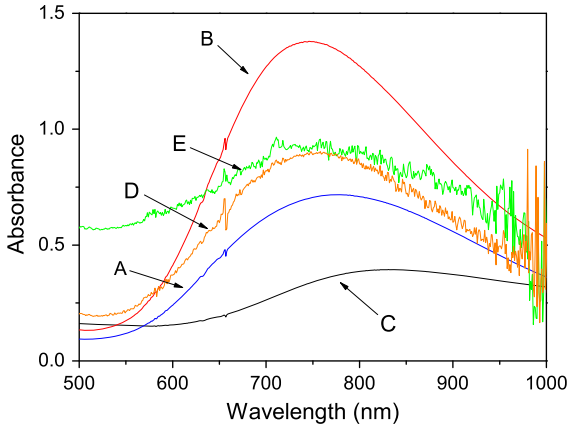

Fig. 8 Vis-NIR spectra of the chitosan (*A*), gelatin (*B*), agar blends (*C*) and chitosan-gelatin (*D*) and chitosan-agar polyblends (*E*)

approach, it should be noted that the overlapping integral between the *d* orbital of the copper ion and the *p* orbital of the ligand atoms is not negligible; therefore, it is not feasible to precisely indicate the nature of the bonds but only provide trends. The covalency parameter α^2 can be evaluated from the EPR spin Hamiltonian parameters by using the simplified Eq. 2 (Pilbrow 1990; Boobalan and Rao 2010; Kivelson and Neiman 1961),

$$\alpha^2 = \frac{A_{||}}{P} + \left(g_{||} - 2\right) + \frac{3}{7}\left(g_{\perp} - 2\right) + 0.04, \qquad (2)$$

where $P = 0.036\ \mathrm{cm}^{-1}$ is the dipolar hyperfine coupling constant for free Cu^{2+}.

The coefficient β^2 describes the covalency of the in-plane π bonding; the smaller the value of β^2 is, the greater the covalent nature of the bond. It has been previously noted that β^2 is more sensitive to variation in covalency than α^2 and is, therefore, a better indicator of bond character (Boobalan and Rao 2010; Kivelson and Neiman 1961). The β^2 coefficient can be calculated using Eq. 3 (Ganesan and Viswanathan 2004).

$$g_{||} = g_{\mathrm{e}}\left[1 - \frac{4\lambda\alpha^2\beta^2}{\Delta E_{xy}}\right], \qquad (3)$$

where ΔE_{xy} is the energy corresponding to the transition $^2B_{1g} \rightarrow {}^2B_{2g}$, and λ is the spin–orbit coupling constant ($\lambda = -828\ \mathrm{cm}^{-1}$ for Cu^{2+}). Here, ΔE_{xy} was assumed to be the peak energy of the only one absorption observed in the 750–840 nm region of the Vis-NIR spectra (Fig. 8). Using Eqs. (2) and (3), the bond coefficients α^2 and β^2 were evaluated and are given in Table 4. Because of the uncertainty involved in the assignment of ΔE_{xy} and $g_{\perp}$, the calculated values of the bond coefficients are accurate within 5 %. In general, the MO coefficients are smaller than unity, indicating the covalent nature of the bonding between the metal and ligand orbital. The values of α^2 obtained for the studied biomembranes are in the range of 0.83–0.91, indicating moderate covalency for the σ bonding. The β^2 values are in the range of 0.57–0.63 for the gelatin and chitosan blends, indicating that the in-plane π bonding is mostly covalent. The fact that $\beta^2 < \alpha^2$ suggests that the in-plane π bonding is more covalent than the in-plane σ bonding. It is interesting to note that the bonding parameter $\beta^2 = 0.79 \pm 0.04$ obtained for the agar blend (Table 4) is considerably higher than the values found for gelatin and chitosan blends and indicates that the in-plane π bonding is less covalent than in other samples.

In summary, the EPR spectra for the copper ion in the studied samples exhibit a resonance signal that is characteristic of Cu^{2+} ions in tetragonally distorted octahedral sites. The EPR parameters were determined by simulation of the spin Hamiltonian of copper ions in axial symmetry. Finally, the relation $g_{||} > g_{\perp} > g_{\mathrm{e}}$ observed in all the samples is also consistent with the d_{x2-y2} ground state of the Cu^{2+} ion. Different copper species were identified in the EPR spectra, being two for gelatin and chitosan and three for the agar blends.

Conclusions

The present article shows the results from complex impedance spectroscopy, proton nuclear magnetic resonance (NMR) and electron paramagnetic resonance (EPR) of polysaccharide- and gelatin-based blends and polyblends. The best ionic conductivities of 7.9×10^{-5} S/cm at room temperature and 2.5×10^{-3} S/cm at 80 °C were obtained for the chitosan-agar polyblends. The activation energies of 0.58 and 0.48 eV of the chitosan–agar polyblend were calculated from the ionic conductivity Arrhenius plot and the onset of NMR line narrowing, respectively. The onset of the ^1H NMR line-narrowing results were also used to determine the glass transition temperatures (T_g^{NMR}) that varied from 200 to 215 K depending on the membrane composition. The temperature

dependence of the ^{1}H spin–lattice relaxation shows the asymmetrical inverted-V shapes around the relaxation rate maximum. The fitting of these data with the BPP model revealed two distinct proton dynamics: one associated with the protons of the acetic acid and another one caused by protons in different environments, probably in glycerol. The EPR spectra of the studied samples showed a resonance signal characteristic of Cu^{2+} ions in tetragonally distorted octahedral sites. The empirical model of Blumberg and Peisach, which correlates the pair of Cu^{2+} EPR parameters ($g_{\|}$, $A_{\|}$) to the bonding nature of the Cu^{2+} in copper complexes, was used to establish the involvement of nitrogen and oxygen atoms in the copper complexation of the bioblends and polyblends. The results revealed copper ions complexed by nitrogens and oxygens in the membranes containing chitosan or gelatin and only by oxygens in agar-based ones. Moreover, it was reported that the gelatin and chitosan blends possess in-plane π bonding that is less covalent than in other samples. Finally, significant information about the nature of bonding in the Cu^{2+} ion was derived from the magnitude of the covalency parameters. The bonding parameters α^2 indicate a moderate covalency for the σ bond between the Cu^{2+} and its ligand in the chitosan blends.

All these results suggest that natural bioblends and polyblends are interesting systems to use in materials science engineering.

Acknowledgments The financial support of the Brazilian agencies Capes, CNPq and FAPESP are gratefully acknowledged. Research was partially financed by the CeRTEV, Center for Research, Technology and Education in Vitreous Materials, FAPESP 2013/07793-6.

References

Bohmer R, Jeffrey KR, Vogel M (2007) Solid-state LiNMR with applications to the translational dynamics in ion conductors. Prog Nucl Magn Reson Spectrosc 50(2–3):87–174. doi:10.1016/j.pnmrs.2006.12.001

Boobalan S, Rao PS (2010) Structural elucidation of Cu(II) ion doped in hexaaquozincdiaquobis(malonato)zincate host by EPR spectroscopy. J Phys Chem Solids 71(11):1527–1533. doi:10.1016/j.jpcs.2010.07.019

Carl PJ, Larsen SC (2000) EPR study of copper-exchanged zeolites: effects of correlated g- and A-strain, Si/Al ratio, and parent zeolite. J Phys Chem B 104(28):6568–6575. doi:10.1021/Jp000015j

Chanda M, Roy SK (2006) Plastics technology handbook. In, CRC Press, pp 896

Cheng MY, Deng JU, Yang F, Gong YD, Zhao NM, Zhang XF (2003) Study on physical properties and nerve cell affinity of composite films from chitosan and gelatin solutions. Biomaterials 24(17):2871–2880. doi:10.1016/S0142-9612(03)00117-0

Chung SH, Heitjans P, Winter R, Bzaucha W, Florjanczyk Z, Onoda Y (1998) Enhancement of ionic conductivity by the addition of plasticizers in cationic monoconducting polymer electrolytes. Solid State Ionics 112(1–2):153–159. doi:10.1016/s0167-2738(98)00229-x

Ciardelli G, Chiono V (2006) Materials for peripheral nerve regeneration. Macromol Biosci 6(1):13–26. doi:10.1002/mabi.200500151

Cremona M, Legnani C, Vilani C, Calil VL, Barud HS, Quirino WG, Achete CA, Ribeiro SJL (2008) Bacterial cellulose membrane as flexible substrate for organic light emitting devices. Thin Solid Films 517(3):1016–1020. doi:10.1016/j.tsf.2008.06.011

Donoso JP, Cavalcante MG, Bonagamba TJ, Nascimento OR, Panepucci H (1995) Magnetic-resonance study of water-absorption in some peg-lithium salt polymer electrolytes. Electrochim Acta 40(13–14):2357–2360. doi:10.1016/0013-4686(95)00193-I

Donoso JP, Lopes LVS, Pawlicka A, Fuentes S, Retuert PJ, Gonzalez G (2007) Nuclear magnetic resonance study of PEO-chitosan based polymer electrolytes. Electrochim Acta 53(4):1455–1460. doi:10.1016/j.electacta.2007.04.101

Eckert H (1992) Structural characterization of noncrystalline solids and glasses using Solid-state Nmr. Prog Nucl Magn Reson Spectrosc 24(3):159–293. doi:10.1016/0079-6565(92)80001-V

El-Hefian EMA, Nasef MM, Yahaya AH, Khan RA (2010) Preparation and characterization of chitosan/agar blends: rheological and thermal studies. J Chil Chem Soc 55(1):130–136

Ganesan R, Viswanathan B (2004) Physicochemical and catalytic properties of copper ethylenediamine complex encapsulated in various zeolites. J Phys Chem B 108(22):7102–7114. doi:10.1021/Jp037765o

Giua M, Panero S, Scrosati B, Cao X, Greenbaum SG (1996) Investigation of mixed cation effects in PEO(9)Zn(1-x)Cu(x)(CF3SO3)(2) polymer electrolytes. Solid State Ionics 83(1–2):73–78. doi:10.1016/0167-2738(95)00216-2

Gomez-Estaca J, Gomez-Guillen MC, Fernandez-Martin F, Montero P (2011) Effects of gelatin origin, bovine-hide and tuna-skin, on the properties of compound gelatin-chitosan films. Food Hydrocoll 25(6):1461–1469. doi:10.1016/j.foodhyd.2011.01.007

Guo T, Zhao JN, Chang JB, Ding Z, Hong H, Chen JN, Zhang JF (2006) Porous chitosan–gelatin scaffold containing plasmid DNA encoding transforming growth factor-beta 1 for chondrocytes proliferation. Biomaterials 27(7):1095–1103. doi:10.1016/j.biomaterials.2005.08.015

Hathaway BJ, Billing DE (1970) Electronic properties and stereochemistry of mono-nuclear complexes of copper(Ii) ion. Coord Chem Rev 5(2):143. doi:10.1016/S0010-8545(00)80135-6

Hong H, Liu CS, Wu WJ (2009) Preparation and characterization of chitosan/PEG/gelatin composites for tissue

engineering. J Appl Polym Sci 114(2):1220–1225. doi:10.1002/App.30619

Huang Y, Onyeri S, Siewe M, Moshfeghian A, Madihally SV (2005) In vitro characterization of chitosan–gelatin scaffolds for tissue engineering. Biomaterials 26(36):7616–7627. doi:10.1016/j.biomaterials.2005.05.036

Justi KC, Laranjeira MCM, Neves A, Mangrich AS, Favere VT (2004) Chitosan functionalized with 2[-bis-(pyridylmethyl) aminomethyl]4-methyl-6-formyl-phenol: equilibrium and kinetics of copper(II) adsorption. Polymer 45(18):6285–6290. doi:10.1016/j.polymer.2004.07.009

Kadir MFZA, Teo LP, Majid SR, Arof AK (2009) Conductivity studies on plasticised PEO/chitosan proton conducting polymer electrolyte. Mater Res Innov 13(3):259–262. doi:10.1179/143307509x440460

Kadir MFZ, Majid SR, Arof AK (2010) Plasticized chitosan-PVA blend polymer electrolyte based proton battery. Electrochim Acta 55(4):1475–1482. doi:10.1016/j.electacta.2009.05.011

Kivelson D, Neiman R (1961) ESR studies on bonding in copper complexes. J Chem Phys 35(1):149–155. doi:10.1063/1.1731880

Kramareva NV, Finashina ED, Kucherov AV, Kustov LM (2003) Copper complexes stabilized by chitosans: peculiarities of the structure, redox, and catalytic properties. Kinet Catal 44(6):793–800

Kreuer KD (1997) Fast proton conductivity: a phenomenon between the solid and the liquid state? Solid State Ionics 94(1–4):55–62

Lopes LVS, Dragunski DC, Pawlicka A, Donoso JP (2003) Nuclear magnetic resonance and conductivity study of starch based polymer electrolytes. Electrochim Acta 48(14–16):2021–2027. doi:10.1016/S0013-4686(03)00181-6

Mattos RI, Pawlicka A, Lima JF, Tambelli CE, Magon CJ, Donoso JP (2010) Magnetic resonance and conductivity study of gelatin-based proton conductor polymer electrolytes. Electrochim Acta 55(4):1396–1400. doi:10.1016/j.electacta.2009.04.038

Ng STC, Forsyth M, MacFarlane DR, Garcia M, Smith ME, Strange JH (1998) Composition effects in polyetherurethane-based solid polymer electrolytes. Polymer 39(25):6261–6268. doi:10.1016/S0032-3861(98)00153-0

Ogihara W, Sun JZ, Forsyth M, MacFarlane DR, Yoshizawa M, Ohno H (2004) Ionic conductivity of polymer gels deriving from alkali metal ionic liquids and negatively charged polyelectrolytes. Electrochim Acta 49(11):1797–1801. doi:10.1016/j.electacta.2003.12.011

Pawlicka A, Danczuk M, Wieczorek W, Zygadlo-Monikowska E (2008) Influence of plasticizer type on the properties of polymer electrolytes based on chitosan. J Phys Chem A 112(38):8888–8895. doi:10.1021/jp801573h

Pawlicka A, Mattos RI, Lima JF, Tambelli CE, Magon CJ, Donoso JP (2011) Magnetic resonance and conductivity study of a gelatin-based polymer gel electrolyte. Electrochim Acta 57:187–191. doi:10.1016/j.electacta.2011.07.062

Pawlicka A, Mattos RI, Tambelli CE, Silva IDA, Magon CJ, Donoso JP (2013) Magnetic resonance study of chitosan biomembranes with proton conductivity properties. J Memb Sci 429:190–196. doi:10.1016/j.memsci.2012.11.048

Peisach J, Blumberg WE (1974) Structural implications derived from analysis of electron-paramagnetic resonance-spectra of natural and artificial copper proteins. Arch Biochem Biophys 165(2):691–708. doi:10.1016/0003-9861(74)90298-7

Pilbrow JR (1990) Transition Ion Electron Paramagnetic Resonance. Oxford University Press, Oxford

Procter IM, Hathaway BJ, Nicholls P (1968) The electronic properties and stereochemistry of copper(2) Ion. I. Bis(Ethylenediamine)copper(2) complexes. J Chem Soc A 7:1678–1684. doi:10.1039/J19680001678

Raphael E, Avellaneda CO, Manzolli B, Pawlicka A (2010) Agar-based films for application as polymer electrolytes. Electrochim Acta 55(4):1455–1459. doi:10.1016/j.electacta.2009.06.010

Rinaudo M (2006) Chitin and chitosan: properties and applications. Prog Polym Sci 31(7):603–632. doi:10.1016/j.progpolymsci.2006.06.001

Shukur MF, Ithnin R, Illias HA, Kadir MFZ (2013) Proton conducting polymer electrolyte based on plasticized chitosan-PEO blend and application in electrochemical devices. Opt Mater 35(10):1834–1841. doi:10.1016/j.optmat.2013.03.004

Singh BK, Bhojak N, Mishra P, Garg BS (2008) Copper(II) complexes with bioactive carboxyamide: synthesis, characterization and biological activity. Spectrochim Acta A 70(4):758–765. doi:10.1016/j.saa.2007.09.008

Stoll S, Schweiger A (2006) EasySpin, a comprehensive software package for spectral simulation and analysis in EPR. J Magn Reson 178(1):42–55. doi:10.1016/j.jmr.2005.08.013

Stosser R, Sebastian S, Scholz G, Willer M, Jeschke G, Schweiger A, Nofz M (1999) Pulse EPR spectroscopy of Cu2+-doped inorganic glasses. Appl Magn Reson 16(4):507–528

Vedeanu N, Magdas DA, Stefan R (2012) Structural modifications induced by addition of copper oxide to lead-phosphate glasses. J Non Cryst Solids 358(23):3170–3174. doi:10.1016/j.jnoncrysol.2012.08.003

Vieira DF, Avellaneda CO, Pawlicka A (2007) Conductivity study of a gelatin-based polymer electrolyte. Electrochim Acta 53(4):1404–1408

Walderhaug H, Soderman O, Topgaard D (2010) Self-diffusion in polymer systems studied by magnetic field-gradient spin-echo NMR methods. Prog Nucl Magn Reson Spectrosc 56(4):406–425. doi:10.1016/j.pnmrs.2010.04.002

Wilkening M, Bork D, Indris S, Heitjans P (2002) Diffusion in amorphous LiNbO3 studied by Li-7 NMR comparison with the nano- and microcrystalline material. Phys Chem Chem Phys 4(14):3246–3251. doi:10.1039/B201193j

Winter R, Siegmund K, Heitjans P (1997) Nuclear magnetic and conductivity relaxations by Li diffusion in glassy and crystalline LiAlSi4O10. J Non Cryst Solids 212(2–3):215–224. doi:10.1016/S0022-3093(96)00654-0

Wright PV (1975) Electrical conductivity in complexes of poly(ethylene oxide). British Polym J 7:319–327

Yalpani M (1988) Polysaccharides, synthesis, modifications and structure/property relations. Elsevier, Amsterdam

Yu L, Dean K, Li L (2006) Polymer blends and composites from renewable resources. Prog Polym Sci 31(6):576–602. doi:10.1016/j.progpolymsci.2006.03.002

Yu B, Zhou F, Wang CW, Liu WM (2007) A novel gel polymer electrolyte based on poly ionic liquid 1-ethyl 3-(2-methacryloyloxy ethyl) imidazolium iodide. Eur Polym J 43(6):2699–2707. doi:10.1016/j.eurpolymj.2007.03.027